Ceramics International 49 (2023) 14844–14854

Contents lists available at ScienceDirect

Ceramics International

journal homepage: www.elsevier.com/locate/ceramint

Breakdown of the anodized nanostructured anatase for photovoltaic devices: The effect of water content in the electrolyte on preparation of large surfaces of nanotubes

Vilko Mandić [a,*], Ivana Panžić [a], Marijana Kraljić-Roković [a], Mattia Gaboardi [b]

[a] Faculty of Chemical Engineering and Technology, Marulićev Trg 20, 10000, Zagreb, Croatia
[b] Elettra-Sincrotrone Trieste S.C.p.A, Science Area Park, 34149, Basovizza, Trieste, Italy

ARTICLE INFO

Keywords:
Photovoltaic constituents
Nanostructured thin-films
Anatase-rutile-nanotubes
Vertically aligned ordered array
Anodization
Electrolyte
Synchrotron radiation

ABSTRACT

Many researchers are heavily involved in attempts to optimise the course of the electrochemical anodization for preparing nanostructured anatase thin-films. Particularly challenging is to prepare vertically aligned arrays of ordered nanotubes of anatase for application in the photovoltaic (PV) systems which require preparing larger homogeneous crack-free surfaces without the need for pre- or post-treatments. Having previously optimised the anodization cell geometry and electrical settings, here we focus on the electrolyte contribution during the anodization, specifically water content. It was elucidated that the water content can influence the equilibrium and the mechanisms behind several competing processes responsible for the formation of nanotubes (NT): (i) titania formation, (ii) NT formation over intermediate titanium hexafluoride, and (iii) etching of the mentioned phases. We employed broad structural, microstructural, electrochemical, and spectroscopic characterisation tools to shed more light on the development of the system with respect to water presence. Namely, water presence built up conductivity of the electrolyte, and consequently allowed faster oxidation of Ti and subsequently faster etching. Water content increase also facilitated the dissolution of the titanium hexafluoride which is the only water-soluble phase in the system. At moderate water content, the synergy of these processes facilitated: (I) forming the initial titania protective layer (titania prevented short circuits and thus eliminated the need for pre-deposition of protective layers), (II) growth of NT (upgraded the charge transfer), and (III) diminishing the residual nanoformations at the surface of residual titanium oxide or hydroxide phases (fewer nanoformations at surface and fewer residues increased charge transfer and apparent transparency and thus eliminated the need for post-treatment). The highest water content promoted excessive oxidation/etching where first NT with expanded tip were formed (crown-like NT), and then wormholes arose. Similarly, disproportioning in dissolution/oxidation/etching occurred at the lowest water contents resulted in less perfect NTs. The bottlenecks of the whole anodization process were identified proving the feasibility of the compositionally novel preparing procedure for obtaining perfect NT. Specifically for the solar cell application, 12% of water in the electrolyte will facilitate growth of the large-scale crack-free TNTs, with other parameters constant. In the course of the investigation, it was evidenced electrolyte can be utilised as a useful tool for controlling anatase to rutile occurrence and vertical distribution.

1. Introduction

The insight in recent investigations of titanium dioxide shows the material is maybe the most extensively studied semiconducting material with application in areas of solar cells [1,2], gas sensors [3,4], water splitting [5], biological and biomedical applications [6–9] and other. The reason for that lies behind titania abundance, stability, and photoactive electronic structure. In terms of photovoltaic contribution, titania is favourable for the generation, transport, and recombination of photo-induced electron-hole pairs under direct light illumination. Therefore, it is worth considering upgrades of its key parameters like bandgap, photoconductivity and carrier lifetime.

It is already well known that recombination consequences may be reduced by enhancing the texture of the irradiated surface, where the

* Corresponding author.
E-mail address: vmandic@fkit.hr (V. Mandić).

https://doi.org/10.1016/j.ceramint.2022.07.254
Received 10 May 2022; Received in revised form 6 July 2022; Accepted 23 July 2022
Available online 4 August 2022

discovery of 1D materials was shown to be quite promising. 1D TiO_2 nanotube formations were first time successfully prepared using a hydrothermal method by Kasuga [8] and electro-chemically by Zwilling [9,10]. Our focus is the electrochemical potentiostatic process of titania anodization using DC power supply and a platinum counter electrode, which was described in details [11]. The successful anodization of titanium substrate yields unique ordered hollow 1D nanostructures. The tubes display large specific surface area, high mechanical strength, and allow high electron mobility, quantum confinement effects, and direct pathways for fast electron transport through ordered nanotube walls [12,13]. The as-prepared anodized TNTs can be described as a ready-to-use membrane of ordered vertical tubes attached to titanium foil. Their ordered organisation offers functional advantage over randomly distributed tubes achieved by the hydrothermal process [14]. The process often used to achieve ordered titania nanotubes (NT) can be simplified as field-assisted growth and etching over an intermediate phase. It is critical to mention that even nowadays the mechanisms of the anodization process are not without discrepancies, to be specific, the several available theorems only partially describe the full course of the process [13,15–17]. Three simultaneous field assisted processes may be held responsible for the process: (i) oxidation of Ti and formation and growth of titania, (ii) oxide dissolution occurring near metal/oxide interface, and (iii) chemical dissolution of titanium and titania phases, due to etching by fluoride ions, occurring near oxide/electrolyte interface [18,19]. Soon after the start, the metal cations are released and subsequently, compact oxide is formed at the metal/electrolyte interface (Eq. (1)). The processes continues through the oxide layer due to applied voltage [20], yet in presence of the fluoride ions the soluble titanium hexafluoride complex is produced. The literature offers discrepancies from that point. Specifically, it is possible that the titanium hexafluoride complex is formed at oxide/electrolyte and metal/oxide interface as well as the oxide/electrolyte interface (due to direct complexation (Eq. (1))).

$$Ti \rightarrow Ti^{4+} + 4e^- + 2H_2O \rightarrow TiO_2 + 4H^+ + 4e^- \rightarrow TiO_2 + Ti^{4+} + 6HF + 6F^- \rightarrow 2[TiF_6]^{2-} \quad (1)$$

$$Ti^{4+} + (2 + n)H_2O \rightarrow TiO_{2-n}(OH)_{2n} + 4H^+ \quad (2)$$

For the compositional equilibrium, it is important to notice that in the reaction with water or fluoride hydrolysis product; hydroxide ion, the surface may yield: (I) different microstructural parameters due to different growth/etching parameters/conditions, and more important (II) residual titania on all interfaces or hydroxides or oxyhydroxides ($TiO(OH)_2$) on the oxide/electrolyte interface (Eq. (2)) [21,22]. The final porous oxide layer is formed as a result of the continuous process, which involves competition between the chemical dissolution of oxide and anodic oxide formation [23]. At the onset of anodization shallow pores are formed leaving an untreated metallic surface between the pores. Later, as the pores become deeper, the electric field at the untreated metallic regions that stick out increases, enhancing the field-assisted oxide growth and dissolution at the site. This yields the simultaneous formation of pores and voids, i.e. tubular structure [19]. The outcome is a structure consisting of adjacent, parallel, vertically oriented nanotubes, separated from the unreacted part of the foil by a varied thin titania barrier layer. The thickness of the titania layer initially is in the range of titania NT radius [3].

Subsequently, the NT can be annealed at temperatures above 400 °C to yield a primarily crystalline anatase phase, with possible rutile presence primarily at the barrier layer, which may be beneficial for chemical sensors [24–26]. Characteristics of the nanotubes are primarily under the control of the anodization parameters [3,27]. Normally their length may be increased under acidic conditions and voltage, where higher pH values and higher voltages yield longer NT. The wall thickness and pore diameter are also under the influence of anodization voltage as well as anodization electrolyte temperature.

Also for obtaining longer NT, it is necessary to minimize water content in the anodization electrolyte to less than 5%, because water will, among others, favour the dissolution. Excess water may allow increased oxygen gas evolution for the growth of anodic oxide film and in general leads to an exponential increase in electrolyte conductivity [28,29]. Higher water content also leads to oxygen evolution (side reaction) at the anode, which doesn't occur at lower water % but does at higher (above 10%) and can affect the morphology of the NTs, i.e. lead to the formation of the ribs on the outer walls [30]. So the tubes will best grow at optimal water content, whereas the most important question remains: *What is the optimal water content?* Normally literature offers values on the minimum of water necessary for the growth of NT in the EG electrolyte. Water in the minimal amount of about 0.2% is necessary but it is often fixed at still relatively low amount of ~2%. The increase in water % leads to the transition from nanoporous to nanotubular, as well as larger diameter, shorter lengths and thinner barrier layer. While in contrast, an increase in NH_4F leads to a smaller diameter and larger lengths of the tubes. The effect of ammonium fluoride is mainly due to the incorporation of fluoride ions that decrease the barrier layer resistance. An increase in fluoride ions leads also to higher growth rates. In general, it can be said that both increase in H_2O and NH_4F concentration leads to an increase in the chemical attack of the formed oxide layer The different roles of both constituents in the formation of the thin film of titania nanotubes can also be associated with the presence of non-stoichiometric oxides forming during the reaction [29]. A broad investigation of water contents (in the ranges of 1–50%) in anodization electrolytes for titania system shows the majority of authors stick with a safe range of around 2% of water and only scarcely the water is utilised as a major tool for TNT optimisation [31,32].

Findings in the area of optimisation of the anodization parameters are often empirical. Having all other parameters already optimised (such as geometry and power settings), we focus in optimisation of the water content in the fluoride-based ethylene glycol electrolytes, in order to benefit from it (among other growth and etching phenomena in the system). Instead of just offering another optimising of the water content in the anodization electrolyte, this work focuses on understanding the equilibrium between mechanisms responsible for the anodization to successful TNTS and extrapolates the functional performance of the TNTs towards different applications as a function of the wide-range changing of the water content.

2. Materials and methods

2.1. Synthesis

Porous titania structures were derived at room temperature by potentiostatic anodization process in a conventional two-electrode cell (Pt foil as the counter electrode and titanium foil as the anode) using a direct current power supply of 60 V for 180 min on previously 3-step cleaned titanium foils, exposing radial surface in diameter of 1 cm to the electrolyte. For the whole time of anodization, the current was monitored and recorded in the form of I-t graphs. In order to enhance the change of current curves were first derived (d I-t). After anodization, the samples were cleaned using isopropyl alcohol (IPA, $(C_3H_8O$, p. a. Kemika, Croatia) and MilliQ H_2O and dried in a nitrogen gas stream, subsequently samples were later thermally treated under the same conditions of at 450 °C for 1 h with the rate of 2 °C/min to induce titania crystallisation.

The electrolyte was 0.3 wt% ammonium fluoride (NH_4F, p. a. Kemika, Croatia) and 2, 6, 9, 12, 14, 16, 18 and 24 wt% MilliQ water in ethylene glycol ($C_2H_6O_2$, p. a. Kemika, Croatia). The only process parameter different was the water content in the electrolytes. Anodization parameters are given in Table 1, while the process scheme is given in Fig. 5a. Samples were denominated as PtW2, PtW6, PtW9, PtW12, PtW14, PtW16, PtW18 and PtW24 (Table 1).

Table 1
Anodization parameters and sample denomination.

Ti-foils	Anodization				Electrolyte		Heating	
	Voltage /V	Time /min	Temp. /°C	Diam. /cm	MilliQ /wt%	NH_4F /wt%	Dwell /°C	Rate/°C/min
PtW2	60	180	22	1	**2**	0.3	450	2
PtW6	60	180	22	1	**6**	0.3	450	2
PtW9	60	180	22	1	**9**	0.3	450	2
PtW12	60	180	22	1	**12**	0.3	450	2
PtW14	60	180	22	1	**14**	0.3	450	2
PtW16	60	180	22	1	**16**	0.3	450	2
PtW18	60	180	22	1	**18**	0.3	450	2
PtW24	60	180	22	1	**24**	0.3	450	2

2.2. Characterisation techniques

IR spectra of the electrolyte samples were recorded using the Fourier transform infrared spectrometer Bruker Vertex 70 in ATR (attenuated total reflectance) mode. The absorbance data was collected between 400 and 4000 cm^{-1} with a spectral resolution of 1 cm^{-1} and an average of 64 scans. The obtained spectra were deconvoluted using Gaussian peak function in order to assign the specific bands.

Grazing incidence X-ray diffraction (GIXRD) measurements were performed on the thin films samples at the Material characterisation by X-ray diffraction beamline (MCX) of the Elettra synchrotron radiation facility (Trieste, Italy), on a Huber 4-axis goniometer equipped with a fast scintillator detector in grazing incidence setup (GIXRD) using 2.4 GeV synchrotron radiation, with an incident beam energy of 8 keV (corresponding to CuKα1 radiation). The thin film samples were fixed on flat sample holder and adjusted on position using theta-scan and z-scans. Patterns were collected in a broad °2θ range, with steps of 0.01°2θ, collecting time of 1 s per step, and incidence angles from 0.25 to 3.00°θ, at ambient temperature and relative humidity of 20%. Diffraction data embed signals from surface beyond the anodized region.

Morphology of the surfaces was investigated using field emission gun scanning electron microscopy (FEG-SEM) device JEOL model 7000F equipped with an energy dispersive spectroscopy (EDS) system.

Cyclic voltammetry (CV) and electrochemical impedance spectroscopy (EIS) were used to compare the electrolytes. The cyclic voltammograms were recorded first in mixtures of common electrolyte and anodization-bath electrolytes under a wide potential range to determine the optimum. Finally, CV spectra were recorded using a EG&G M263A potentiostat in anodization-bath electrolytes in a potential range −1 to 1 V at the scan rate 0.05, 0.10 and 0.20 Vs^{-1}. All scans were repeated 3 times. The EIS spectra were taken in the same solutions at potentials corresponding to the current peak obtained during the positive direction sweep. The superimposed sinusoidal voltage signal of ±5 mV amplitude was applied. Data were collected within the frequency range of 10^5 to 10^{-2} Hz, taking five points per decade. For impedance measurements, PAR lock-in amplifier M5210 was used in the combination with the potentiostat M263. The three-electrode setup was used with Pt as the working electrode (A = 0,07 cm^2), Ag/AgCl reference electrode and Pt-foil (2 cm^2 area) as an auxiliary electrode. All potentials in this work are quoted in reference to Ag/AgCl electrode.

3. Results and discussion

3.1. Spectroscopic characterisation as a function of electrolyte composition

The IR scans of all different electrolytes (not the anodized films) were recorded in ATR reflectance mode (Fig. 1). We analysed freshly prepared electrolytes and the electrolytes after use in the anodization experiment. The idea was to get a better understanding of the possible changes in the electrolyte composition and the subsequent effect on the resulting NTs parameters. Scans show bands typical for ethylene glycol and water

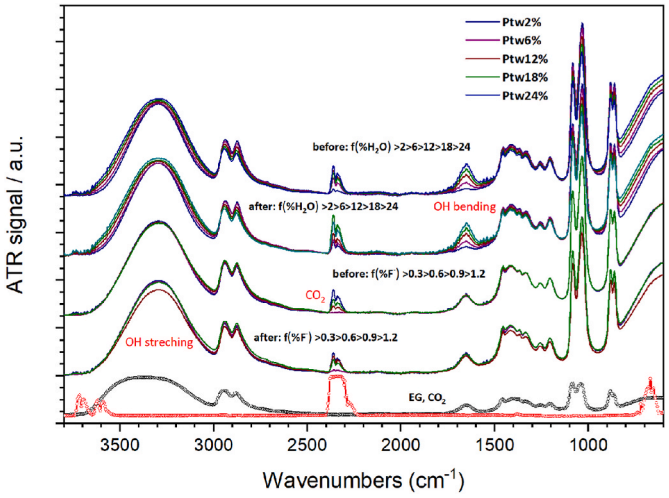

Fig. 1. ATR FTIR scans of the selected fresh electrolytes and electrolytes used for anodizations.

presence while bands for ammonium fluoride were noticed only in traces [33,34]. Interestingly, carbon dioxide bands were observed as well [35]. The abovementioned was expected for the fresh and used electrolytes. No frequency shifts were observed. However, the observed intensity of the bands related to water and EG suggests that with the increase of water content, the intensity of ethylene glycol bands decreased, while the intensity of ammonium fluoride remains unaffected. As expected, the trend of the intensity increase of the bands related with water (OH stretching and bending) follows water content increase. In addition to that, with water content increase, a stronger intensity of carbon dioxide bands was observed. Having the above-mentioned in mind it may be interesting to look further into the role of carbonaceous constituents of the electrolyte on the electric behaviour. Namely, the differences in the course of the electrochemical dissolution of the ethylene glycol phase as a function of the water content may be responsible for the differences in the mechanisms of the electrochemical growth of the titania nanoformations. This will be further examined by voltammetry measurements.

The addition of water (even considerable amounts of water) to the electrolyte do not induce any fundamental changes of the electrolyte, as shown by the FTIR spectra. From the FTIR point of view, electrolytes recorded before use and after use show no significant differences. This may suggest electrolytes can be considered stable and used for multiple anodizations. However, FTIR results do suggest that the increase of water content in the electrolyte influences the electrical mobility of species in the system by means of affecting the dissolution capabilities of certain constituents, most probably the intermediate titanium hexafluoride. Namely, the differences in the yield nanoformations can be reasonably explained only in the case of titanium hexafluoride being affected by the water-governed changes of the electrolyte system, which

were expected due to the solubility of titanium hexafluoride in water [30].

3.2. Electrochemical characterisation as a function of electrolyte composition

Normally researchers try to demystify the behaviour of the system during the course of processing that is not completely known. In order to mitigate any uncertainty during the titanium anodization we refer to platinum working and reference electrodes. Namely, titanium anodization is always a somewhat ambiguous process while by using 2 Pt electrodes we should avoid such uncertainty. Therefore, any interesting phenomena observed must be the consequence of the medium used, i.e. electrolytes with different compositions. So, we investigated the electrolyte properties by using CV method and platinum working electrode (Fig. 2).

From the obtained results it is evident that at potentials more positive than 0 V two anodic current peaks are formed. The positive sweep peak, registered from 450 mV to 340 mV, is related to EG oxidation while the current increase above 600 mV represents EG oxidation at oxidised Pt surface. The negative sweep peak, registered from 450 mV to 0 mV, is related to the oxidation of EG at the activated platinum surface following the reduction of platinum oxide [36–39]. The CV results indicate that the current values of positive and negative sweep peaks increase by water addition up to 18% (Table 2). This behaviour is a result of higher rate of EG degradation in the solution that is characterised by better conductivity. However, the amounts of water higher than 18% decrease EG degradation rate and consequently the corresponding current. The electrolyte resistance also influences the potential of the current peak in the positive sweep direction, and by water addition the potential decreases. The trend is less regular for negative sweep peak. The current obtained at potentials more negative than 0 V is

Table 2
Current and potentials for CV measurements at different scan rates.

water content	20 mV s^{-1}		10 mV s^{-1}		5 mV s^{-1}	
	E_p/mV	I_p/mA	E_p/mV	I_p/mA	E_p/mV	I_p/mA
2%	218	0.006	191	0.004	209	0.002
	533	0.030	516	0.021	507	0.014
6%	163	0.007	174	0.003	220	0.001
	493	0.040	449	0.019	476	0.012
9%	191	0.008	177	0.007	151	0.006
	489	0.041	467	0.032	463	0.025
12%	244	0.019	189	0.011	147	0.007
	533	0.062	524	0.043	465	0.025
14%	231	0.033	191	0.013	102	0.005
	493	0.075	478	0.046	507	0.024
18%	302	0.048	183	0.018	138	0.009
	571	0.116	485	0.063	462	0.043
24%	236	0.017	120	0.01	130	0.005
	493	0.075	475	0.050	449	0.02

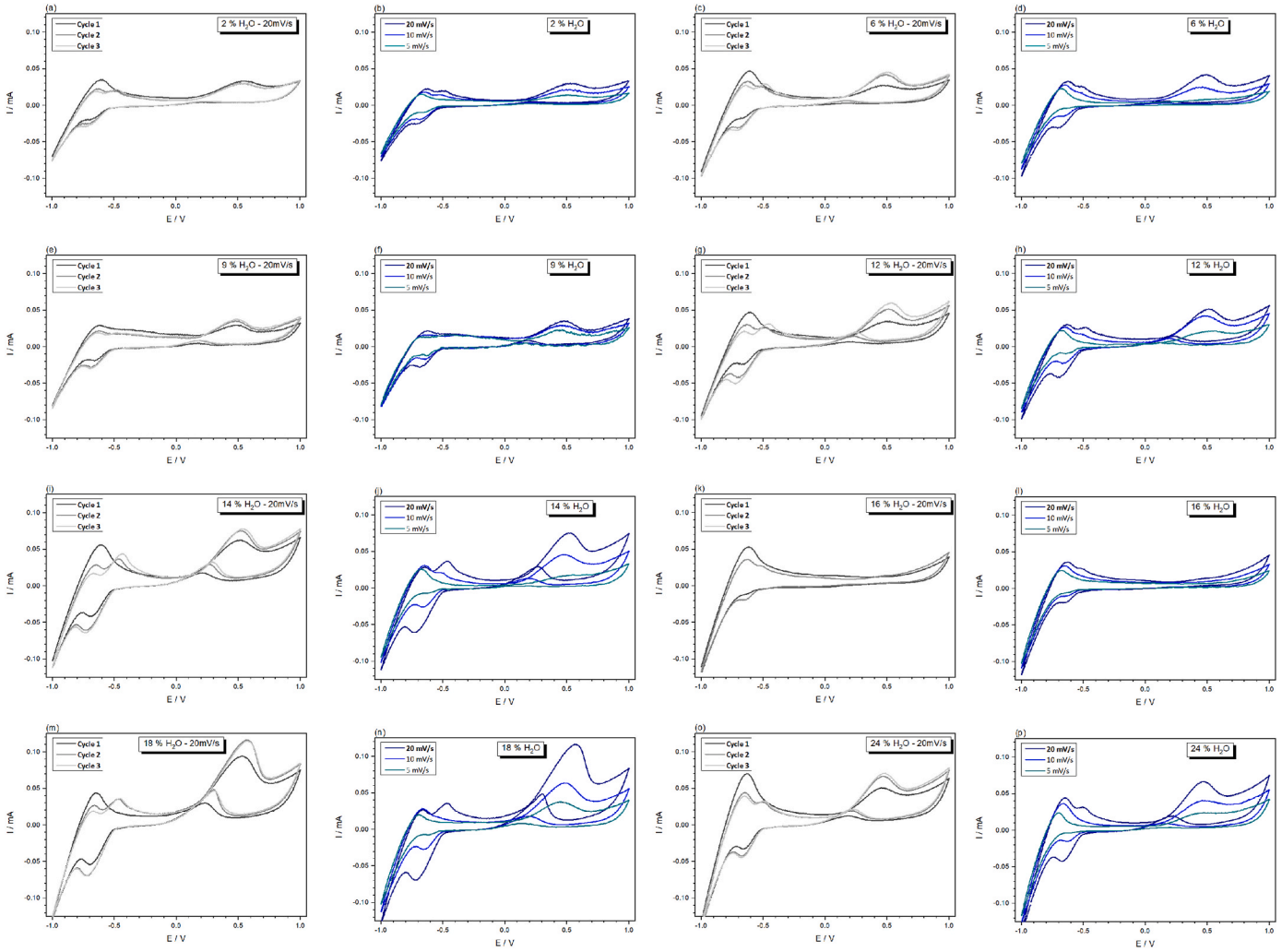

Fig. 2. Cyclic voltammetry results. For each electrolyte containing; (a,b) 2% of H_2O; (c,d) 6% of H_2O; (e,f) 9% of H_2O; (g,h) 12% of H_2O; (i,j) 14% of H_2O; (k,l) 16% of H_2O; (m,n) 18% of H_2O; (o,p) 24% of H_2O first we show 3 cycles taken at a rate of 20 mV s^{-1}, and then comparison of the 3rd scan for rates of 5, 10 and 20 mV s^{-1}.

related to redox reaction of hydrogen. As evident hydrogen redox reaction current decreases by cycle number due to platinum poisoning by CO [40]. The best scan rate in terms of the resolution was 20 mV s^{-1}, which is expected for the solution-type fast processes.

CV results are supported by EIS results (Fig. 3), charge transfer resistance decreases up to 18% water, and for the amounts of water higher than 18%, it increases again. On the other hand, electrolyte resistance decreases from 2% to 24%. The diameters of impedance arcs represent charge transfer resistance and the first intersection of the semicircle represents the electrolyte resistance. The IS scans confirm the water is contributing to the charge transfer effect in the electrolyte. The mobility of the charge-carrying species increases with the water content, thus electrolytes show higher conductivities.

3.3. Structural characterisation of TNTs as a function of the electrolyte composition

The electrodes (anodized foils) prepared using different electrolytes were first structurally characterised at a synchrotron facility by means of grazing incidence X-ray diffraction at various incidence angles from 0.25° to 3.00° theta (Fig. 4). Structural characterisation normally enables qualitative determination of the average crystalline composition. In the GIXRD setup the change of incidence angle enables depth profiling of the samples, i.e. the crystal composition may be monitored as a function of the depth qualitatively, but also with some semi-quantitative information. Normally, for the thermally treated samples the expected composition near surface is porous titania while in-depth dense titanium. When we specifically talk about TNT formation then the porous titania actually consists of three layers: (i) a thin titania layer at the bottom, (ii) following layer with long ordered TNT, and (iii) finally porous titania on top. However, is seems that the different compositions of electrolytes used in anodization promotes somewhat different yields of the mentioned titania layers. Basically, the composition of the titania at the top can be changed, the thickness of the titania that reposes in the middle can be changed, and the occurrence or observation of the titania that reposes at the bottom is conditional. Under moderate thermal treatment conditions (450 °C for 1 h) all titania layers should crystallise to anatase (with possibly some rutile). It is not possible to differentiate between them by means of volume average diffraction. Therefore, it is important to utilise the depth profiling capability of the GIXRD to shed more light at the system.

The most important observation arises as a consequence of the

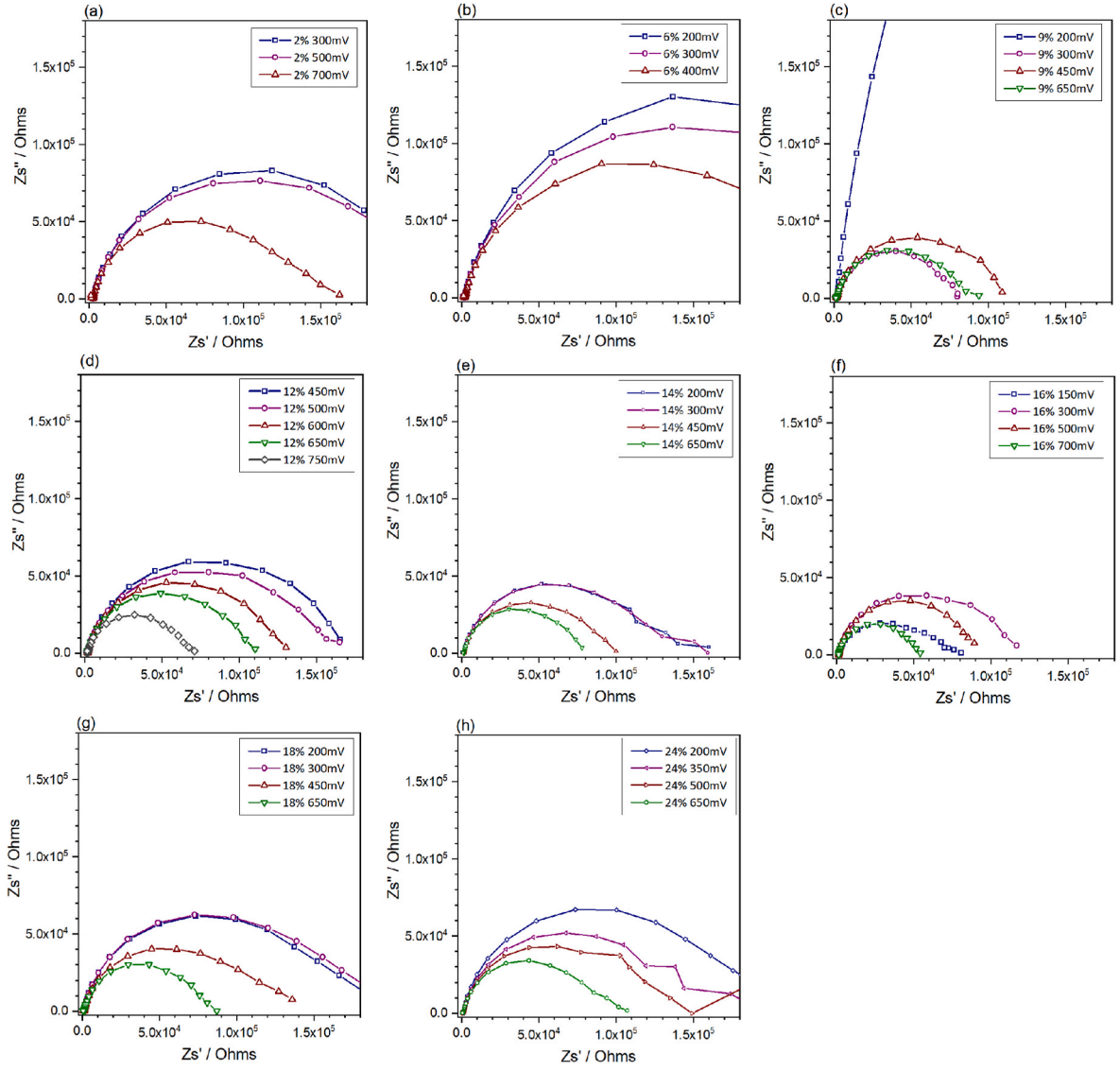

Fig. 3. Complex plane impedance plots of Pt electrode in EG containing different amount of water at potentials in the range from 150 to 700 Mv, for electrolytes containing; (a) 2% of H_2O; (b) 6% of H_2O; (c) 9% of H_2O; (d) 12% of H_2O; (e) 14% of H_2O; (f) 16% of H_2O; (g) 18% of H_2O; (h) 24% of H_2O.

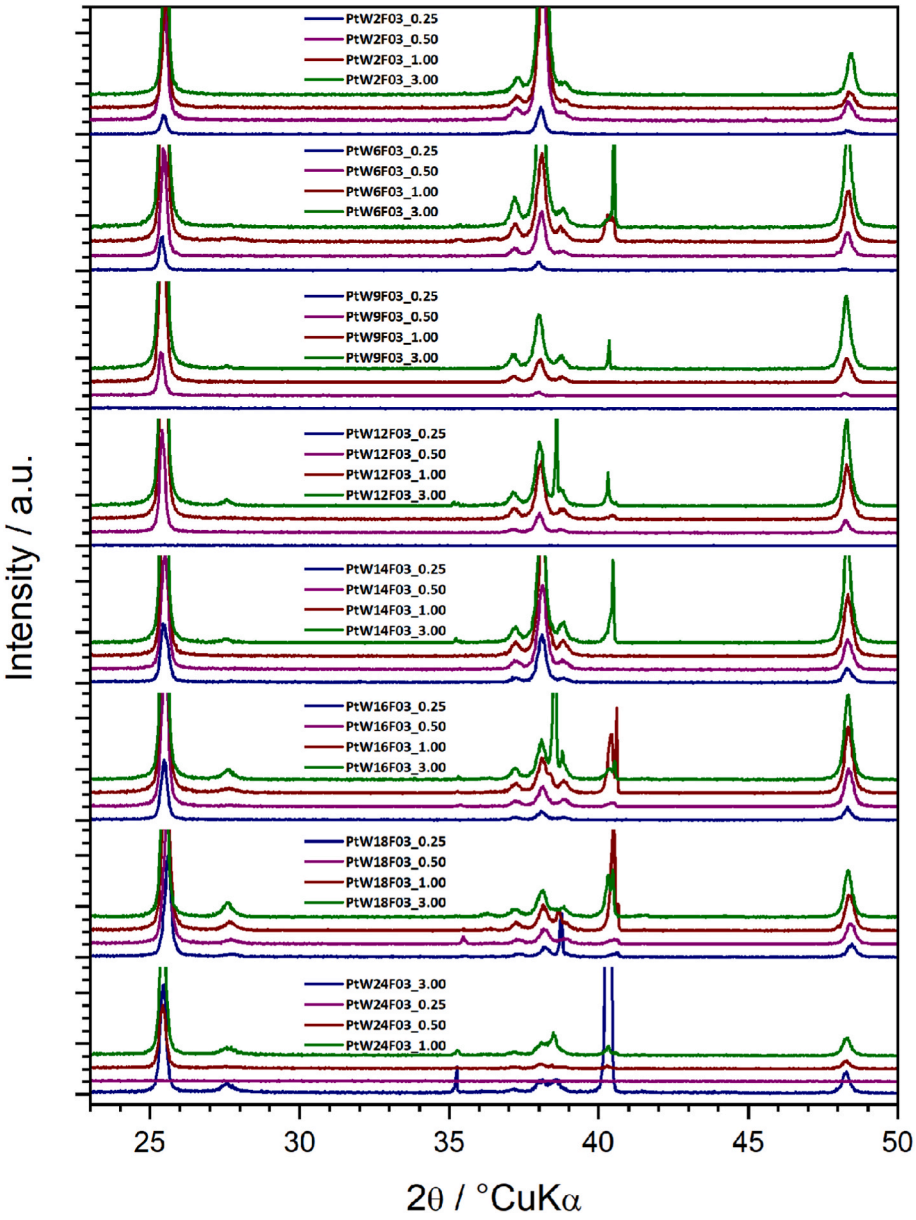

Fig. 4. Synchrotron quality of GIXRD scans for all thin-film samples at different grazing angles.

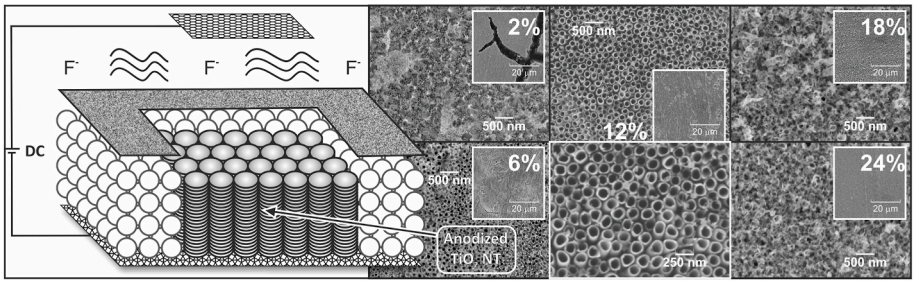

Fig. 5. Left to right; scheme of the anodization at titanium foil; high magnification FESEM micrographs of the investigated films prepared using electrolytes containing 2, 6, 12, 18 and 24% of H_2O; low magnification FESEM micrographs were added as insets to illustrate macroscopic quality of the film surface.

different anodization conditions that may yield oxygen-deficient or oxygen-rich surface titania layer. Therefore, the possibility of formation of for example titania hydroxides or oxyhydroxides is monitored. The species were however not observed (at least the crystalline species were not observed). The confirmed phases in the system are titanium (**ICDD PDF#44–1294**) anatase (**ICDD PDF#21–1272**), and rutile (**ICDD PDF#21–1276**).

At a grazing angle of 0.25°θ (which collects information only from the very top surface) all samples yield only anatase pattern resembling surface-based porous-layer. The only samples that do not show any

pattern at this angle are samples **PtW9** and **PtW12**. This actually points out that the tips of the TNTs are substantially flat and almost completely free of porous-surface-titania. Such a flat top surface actually shows the 0.25° theta actually is lower than the grazing angle for a layer that is equivalent to a planar layer. As previously explained in the introduction such accessible TNT are interesting for photovoltaic application (easier infiltration, better transparency, cumulatively higher solar cell efficiency). Obviously, the top titania is negligible upon anodization in electrolytes containing near **12%** of water, while for any higher or lower water contents it is clearly present. If anywhere, one would expect to find some titania hydroxides or oxyhydroxides in this case. Yet, the presence of the above-mentioned phases was not confirmed, however, their presence cannot be excluded beyond a reasonable doubt. Namely, they may exist in minute quantities in very thin nanometre-thick layer which surpasses the resolution of the diffraction setup, or their organisation is not crystalline.

At grazing angles of 0.5°θ and 1.0°θ (which collects information from the surface and slightly below) anatase is the dominant phase in all samples. This pattern primarily arises from TNT or TNT-like structures. One can observe that for samples anodized in electrolytes containing between **6** and **18**% of water (so for low and high quantities) titanium pattern emerges. That points out to higher thickness of the nanostructured anatase in samples anodized in electrolytes containing nearly **12**% of water. Obviously hierarchical growth of 1D tubular structures allows for achieving higher thickness in comparison to non-hierarchical growth of isotropic porous structures.

Titanium is continuously observed in all samples at an angle of 3°θ. This angle definitively allows monitoring of the bottom titania layer. Interestingly, for all samples here we observe also the rutile phase. Normally such phase is not expected upon thermal treatment at 450 °C for 1 h, yet thermodynamic conditions crystallisation may have obviously been fulfilled locally [41,42]. Again samples near **12**% (**PtW9**, **PtW12,** and **PtW14**) show rutile only at an angle of 3°θ while **PtW6** at 1 and 3°θ, **PtW18** on all angles. The strong conditions obviously favour not only to the local formation of rutile. The presence of titanium throughout the sample **PtW18** probably can be attributed to the bent substrate. Also at an angle of 0.5°θ a non-assigned peak occurs. It can be said that the rutile presence is obviously initiated from the in-depth of the sample. The higher the water content the more rutile will be evidenced near the surface. Also higher the water content the more rutile will be semi-quantitatively evidenced. It is well known that anatase with some rutile can boost charge transfer and derivatively boost efficiencies of the systems that utilise such behaviour. Therefore, the ability to control the rutile presence may actually be a much more interesting tool for controlling the system performance in comparison to the existence and properties of the oxygen-deficient or oxygen-rich surface titania layer (for example titania hydroxides or oxyhydroxides), which obviously cannot be easily controlled.

3.4. Microstructural characterisation of TNTs as a function of the electrolyte composition

Electron microscopy micrographs show the typical appearance of several NT samples prepared using electrolytes with different water contents. All samples resemble to titania NT, and differ in homogeneity, uniformity, geometry, residuals and decomposition. One can observe a trend in how certain TNT parameters change with varying the water content (Fig. 5). It can be confirmed that water content in electrolytes contributes to the increase in the NT diameter.

First, at the lowest water content (sample **PtW2**) well-formed ordered NT appears to be covered with so-called residual nanoformations at the surface (Fig. 5). The residual nanoformations at the surface do not have exact chemical composition. The composition is often attributed to titanium oxyhydroxides [11] but actually may be considered a mixture of titanium oxide and titanium hydroxide as previously shown by EDS (Fig. 6). This material has comparatively low mechanical properties and

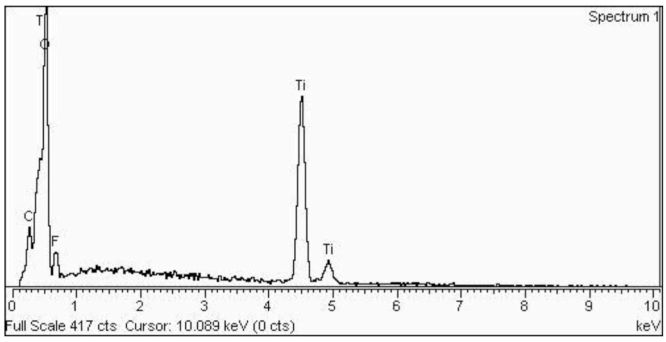

Fig. 6. EDS profile for a selected sample.

it is normally removed by ultrasonic tip previous to photovoltaic application.

The residual nanoformations at the surface reduce dramatically at a water content of **6**% (**PtW6**) revealing more homogeneous surface with NT. Defects exist scarcely at macroscale while at microscale somewhat wider NT are not really uniform.

At a water content of **12**% (**PtW12**) the surface and NT resemble perfectly ordered uniform and homogeneous NT without any debris or residual nanoformations at the surface. Fig. 5 depicts exactly how desirable NT should look. Shown NT are approximately 150 nm in outer and 120 nm in inner diameter and 1500 nm in length. The specific surface of the tubes was approximated to be more than 50 cm^2 cm^{-2} (surface area of hollow cylinder normalised over surface $SS = n_{TNT} \cdot 2\pi \cdot [(R + r) \cdot h + (R^2 - r^2)/2]$.

At a higher water ratio (**18**%) other features will dominate, and this is the decomposition of the NT, starting from the top, yielding a crown-like NT. In the case of control over the process, crown-like microstructure may be favourable due to increased specific surface. The surface is very rough yet homogeneous.

That cannot be said for the morphology which appears at the highest water content (**24**%), which resembles wormhole microstructure, as NT does not form at all or decompose completely. The surface roughness gets reduced and remains homogeneous.

In Fig. 6 residual nanoformations at surface were indicated with EDS. Having in mind the emission of the characteristic X-rays takes place from considerably large volume of the samples, the similarity of all spectra comes as no surprise. We can only confirm general (titanium and oxygen as well as traces of fluoride from the electrolyte) elemental composition, while for further differentiation of the specific surface features, the EDS method doesn't offer sufficient spatial nor energy resolution, and therefore doesn't allow sample cross-correlation.

3.5. Anodization curves and derivative anodization curves

The current density and the water content of the electrolyte affected the O:F atomic ratio and the ionic transport in the films [43]. The electrolyte behaviour is important for TNT growth, namely one can say that ion conduction is responsible for the growth of an oxide, while electron conduction is responsible for the availability of the oxygen from the anode surface.

When we start the anodization process and the initial porous titania layer is formed, the transferring of the electrons becomes impossible. The remaining ion conduction dominates the flow of the current. The field distribution is the function of the surface morphology. The thin bottom titania layer may increase the strength of the field locally and thus increase current density which consequently allows the growth of the pores. Namely the simultaneous oxidation and dissolution processes are field-enhanced. As fluoride ions diffuse through the oxide layer faster than the oxygen ions [30] a boundary layer is formed near the metal-to-oxide interface, resembling water-soluble fluoride-rich layer. Thus, nanoparticles from that area can easily dissolute and further

enhance gaps between them, and facilitate the shift from the porous to tubular morphology [32]. To reach the conditions for stable self-organisation, competing processes have equally shared anodic current to reach equilibrium [30,32].

That does not happen all the time, whereas inhomogeneities occur when the electric field is perturbed and the balance of dissolution and oxidation is disrupted. The properties of the electrolyte are critical in the mitigation of disruptions. While the decrease of the viscosity of the electrolyte by the addition of the water does cause higher diffusivity, on the other hand, it decreases the current densities making the process more diffusion controlled.

The growth of the NT can be monitored using current-time curves obtained during anodization (Fig. 7). I-t curve at a water ratio of 2% should resemble common anodization curve in the case of perfect NT growth, which is not the case here. Namely, a relatively low starting current is an indicator that the charge is poorly delivered to the sample which is due to electrolyte properties. In a few moments the resistance increases due to the formation of titania layer, which serves as a resistor (and electric field enhancer). Very gradual decay points out in relatively controlled average etching of the titanium at the scale of the whole exposed surface, but noisy signal points out in charge transfer differences at the local level primarily on behalf of the differences in local titanium microstructure. Subsequently, In the case of Ti thin films, some current increase may be observed. This occurs as the Ti is almost breached, and normally is considered as one of the indicators the anodization should be stopped. Here we basically observe low onset current and a noisy but continuous moderate decay. Several features change with more water:

(i) **First**, linear increase of onset current may be observed with water content increase, pointing out water increases total mobility of the species in electrolyte, i.e. increases effectivity of the electrolyte as more charge can be delivered to the sample surface.
(ii) **Second**, the period where current remains relatively high gets shorter with water content. More charge will induce abrupt formation of the titania at surface, whereas less time is required for related increase of surface resistance.
(iii) **Third**, the more the water, the faster the formation of titania, the strongest is the relative decay of current due to increase of resistance. This is better visible from the anodization curve derivatives (Fig. 8).
(iv) **Fourth**, is maybe the most critical part of the NT anodization; it can be considered as the inflection point (or even section of the constant current) after the stronger current decay due to titania layer formation.

At this point it is worth mentioning that all anodization basically comprises three processes; (a) one is the formation of titania layer; (b) second is the formation of titania NT over intermediate titanium hexafluoride phase and (c) the third is the etching of the titania phases (dissolution of intermediate phase including). The NT anodization basically requires onset titania and etching conditions, so it may be concluded that the margin of parameters where the NT anodization process will dominate is narrow. As primary parameters influencing the outcome of electric conditions, electrode geometry, and electrolyte composition are nominated. With all other parameters constant, the water content in electrolyte may influence two things.

a) First, the higher water content may increase the mobility of the charge carriers in the electrolyte, subsequently delivering more charge to the sample surface, intensifying first the titania formation and subsequently the etching conditions.
b) Second, the higher water content might facilitate the dissolution of the only water soluble species in the system, the titanium hexafluoride. Previously we observed the occurrence of the change in conductivities of the electrolytes with different amounts of water, which suggests synergy of both mechanisms. This complex behaviour may be simplified as follows.

In lower water curves (2%) the anodization process is long and noisy. The oxidation-growth and the oxidation-etching are normally considered to be continuously competing processes. Here the processes hardly interfere; basically allowing simultaneous and barely dependent growth of NT as well as residual titania oxyhydroxides. The process can be considered non-equilibrium. This consequently yields NT and titania based residuals on top (and bottom). Considerable underlying titania may contribute to macroscopic cracking, as shown in Fig. 9a. On behalf of charge penetration due to cracks, the current remains until the end of the process.

With water increase (6%) the constituent processes can already be distinguished. A more potent electrolyte will allow faster oxidation. This shortens the constant current stage (first of all this prevents thick underlying titania and thus prevents cracks) and subsequently the NT anodization dominates over titania formation. Finally, NTs are faced with less residual titania material, yet the NT achieved are still not macroscopically homogeneous and microscopically uniform (minor current remain).

Further increase of water (12%) yields the optimum conditions for

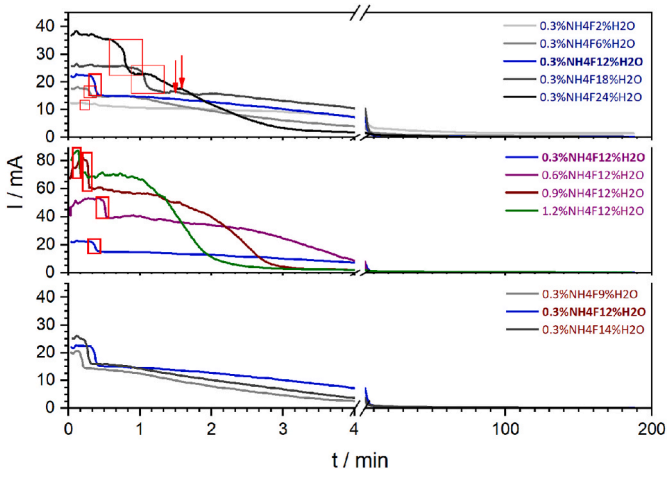

Fig. 7. It curves for anodization for all TNT thin film arrays; top figure – shown as a function of the water content in a broad range, middle figure – shown as a function of the fluoride content, bottom figure – shown as a function of the water content in a narrow range (near optimal).

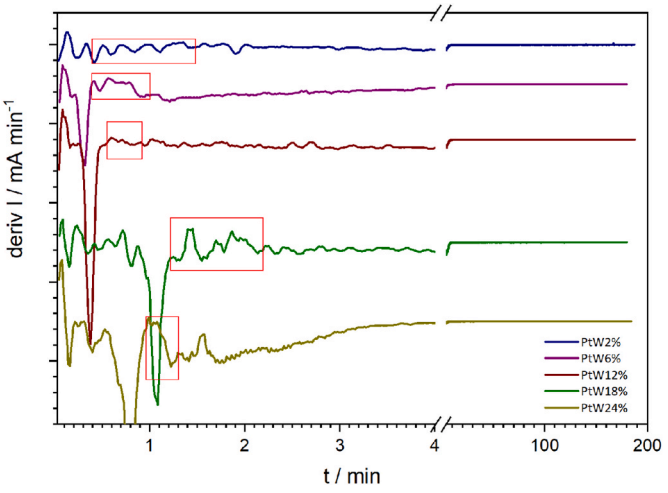

Fig. 8. Derivation DIt curves for anodization for selected TNT thin film arrays.

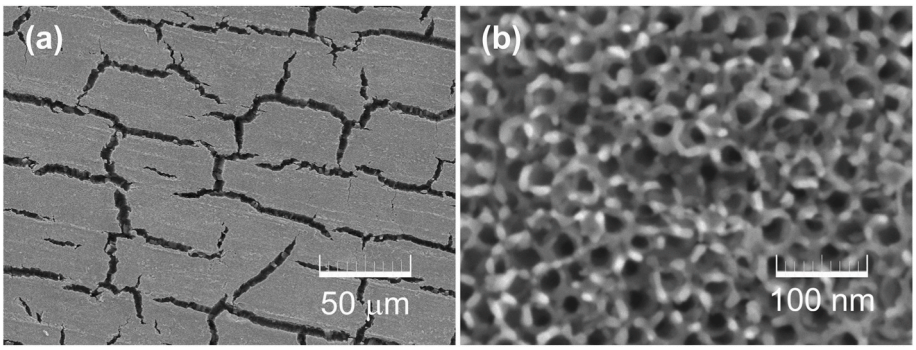

Fig. 9. (a) FESEM micrograph showing an example of macroscopic defect; (b) FESEM micrograph showing an example of wormhole microstructure at highest water content.

NT growth. Almost immediately after the onset titania layer has been formed the NT anodization dominates over titania formation and excess etching. The constant current stage is infinitesimal (actually only an inflection point) and obtained NT's are perfect (homogeneous and uniform). The process was stopped after the current reached minimum values.

More water (18%) reduces the previously established anodization equilibrium. First, it takes a longer time for the titania layer to grow (and increase resistance). Then it takes long time until anodization stabilizes. Finally, the subsequent etching process (of both titania and NT) will be the dominating mechanism over the onset titania layer formation and the NT anodization. Specifically, it seems that all of the stages of the constituent processes (including the intermediate stage of the constant current) increase as each of them can hardly dominate, while finally, the etching phase of the process dominates. Distorted NT will form. With some luck, this lack of control may be shown as favourable for additional NT specific surface increase due to flower like endings. However, this is hardly reproducible. Here we observe some residuals on top but this time not the resisting titania oxyhydroxides type, only the NT debris. This residual cannot be easily removed with post-treatment. There is no residual resistance.

Finally, the highest water content (24%) allows domination of the etching where only a small intermediate constant current stage is observed. Titania is formed fast and anodization occurs only locally. The wormhole-like structure is obtained rather than NT. Homogeneous uniform not ordered porous microstructure is formed, the resistance of the layer is high quickly. Electrolyte is too potent. High-resolution FESEM micrograph from Fig. 9b allows observing of wormhole microstructure at the highest water content.

(v) **Fifth,** for lower water content the current decay does not reach the minimum. This occurs on behalf of the non-equilibrium anodization.

In other words, some titania or titania hydroxide residual nanoformations at the surface are formed on top of already formed NT and act as a resisting layer further interfering with anodization process. This layer was found as unwanted for the SC application and is commonly removed using an ultrasonic tip due to comparatively weak mechanical properties. Despite evidenced success in removal is it still unwanted and points out in a non-equilibrium process.

The geometry properties of just the as-obtained nanotubes were compared with the literature [43–45]. Something like 3% of water was reported as a content where tube length reduces and where inner diameter grows. The roughness of the nanotube walls reduces at somewhat higher water content. The results are only to an extent comparable with ours, due to the specific details of the reactors and particularly large water content range we investigated. The fluoride content also affects NT growth, where first of all small and high fluoride diffusion prevent NT formation, while an increase of the moderate fluoride acts similarly as the water content increases. This is something we will report next. While we focus at the overall properties of the as-formed composite, including other layers and not just the nanotubes, observation of just the nanotube-related behaviour suggests that the properties follow the reported behaviour. However, we think that we addressed a much more comprehensive level of the changes.

Finally, having in mind acidic environment promotes titanium oxide while basic titanium hydroxides it would be interesting to see if promoting basic conditions would reduce the bottom titania layer and therefore reduce cracking, or if promoting acidic conditions would reduce transient titanium oxyhydroxides at the top and therefore reduce the presence of debris.

4. Conclusions

The anodization procedure for the preparation of ordered nanotubes of anatase for the photovoltaic application has been optimised to yield large homogeneous crack-free surfaces without the need for pre-or post-treatments. Having previously optimised the electric conditions and cell geometry, here we focus on the electrolyte properties, specifically water content.

The water content generally can influence the equilibrium of the several competing processes responsible for the NT formation: titania formation, NT formation over intermediate titanium hexafluoride, and etching of the phases.

Water increase adds to the conductivity of the electrolyte consequently allowing faster oxidation of Ti and subsequently etching. Also, water increase contributes to the dissolution of the only water-soluble phase in the system; the titanium hexafluoride.

At moderate water increase, these processes facilitate the initial titania protective layer formation (prevents short circuits and thus eliminates the need for pre-deposition of protective layers), facilitate NT growth, and diminish the residual nanoformations at the surface of residual titanium oxide or hydroxide phases (increases charge transfer and transparency and thus eliminates the need for post-treatment).

The highest water content promotes excessive oxidation/etching where first NT with expanded tip (crown-like NT), and then wormholes arise.

Structural and microstructural characterisation of the NT's and electrochemical and spectroscopic measurements of the electrolytes were used to identify mechanisms and bottlenecks of the anodization; the exact preparation procedure of perfect NT is enclosed.

Interestingly, the tailoring of the electrolyte via water content proved less useful tool for control of the presence of oxygen-deficient or oxygen-rich surface titania but proved very useful for the control of the anatase with some rutile presence and vertical distribution.

Declaration of competing interest

The authors declare that they have no known competing financial interests or personal relationships that could have appeared to influence the work reported in this paper.

Acknowledgement

This work has been funded by the projects PZS-2019-02-1555 PV-WALL in Research Cooperability Program of the Croatian Science Foundation funded by the European Union from the European Social Fund under the Operational Programme Efficient Human Resources 2014–2020 (titania nanotubes for PV systems), UIP-2019-04-2367 SLIPPERY-SLOPE (development of diffraction experiment), of the Croatian Science Foundation, project KK.01.2.1.02.0316 by the European Regional Development Fund (ERDF) (investigation of thin-films). The financial sustenance of the University of Zagreb is gratefully acknowledged. The MCX beamline at Elettra Synchrotron in Trieste is gratefully acknowledged for collaboration under project 20175490. The authors appreciate Domagoj Belić for his assistance in FESEM microscopy and collaborators from RBI fruitful discussions.

References

[1] B. O'Regan, M. Gratzel, A low-cost, high-efficiency solar cell based on dye-sensitized colloidal TiO_2 films, Nature 353 (1991) 737–740, https://doi.org/10.1038/353737a0.
[2] M. Gratzel, Photoelectrochemical cells, Nature 414 (2001) 338–344, https://doi.org/10.1038/35104607.
[3] O.K. Varghese, X. Yang, J. Kendig, M. Paulose, K. Zeng, C. Palmer, K.G. Ong, C. A. Grimes Ca, A transcutaneous hydrogen sensor: from design to application, Sens. Lett. 4 (2006) 120–128, https://doi.org/10.1166/sl.2006.022.
[4] S. Yu, H. Zhang, J. Zhang, Synthesis of high response gold/titanium dioxide humidity sensor and its application in human respiration, Ceram. Int. 47 (2021) 30880–30887, https://doi.org/10.1016/j.ceramint.2021.07.270.
[5] A. Fujishima, K. Honda, Electrochemical photolysis of water at a semiconductor electrode, Nature 238 (1972) 37–38, https://doi.org/10.1038/238037a0.
[6] W.C. Silva, A.C.A. Silva, U. Rocha, N.O. Dantas, W.F. Silva, C. Jacinto, Nd^{3+} doped TiO_2 nanocrystals as self-referenced optical nanothermometer operating within the biological windows, Sens. Actuator A Phys 317 (2021), 112445, https://doi.org/10.1016/j.sna.2020.112445.
[7] C.T. Hardman, H.A. Johnson, M. Doukas, C.C. Pettit, A.V. Janorkar, R. S. Williamson, M.D. Roach, Photocatalytic, phosphorus-doped, anatase oxide layers applicable to titanium implant alloys, Surf. Interface Anal. 54 (2022) 619–630, https://doi.org/10.1002/sia.7074.
[8] K.A. Kravanja, M. Finšgar, A review of techniques for the application of bioactive coatings on metal-based implants to achieve controlled release of active ingredients, Mater. Des. 217 (2022), 110653, https://doi.org/10.1016/j.matdes.2022.110653.
[9] S.S. Samhitha, G. Raghavendra, C. Quezada, P.H. Bindu, Green synthesized TiO_2 nanoparticles for anticancer applications: mini review, Mater. Today Proc. 54 (2022) 765–770, https://doi.org/10.1016/j.matpr.2021.11.073.
[10] T. Kasuga, M. Hiramatsu, A. Hoson, T. Sekino, K. Niihara, formation of titanium oxide nanotube, Langmuir 14 (1998) 3160–3163, https://doi.org/10.1021/la9713816.
[11] V. Zwilling, E. Darque-Ceretti, A. Boutry-Forveille, D. David, M.Y. Perrin, M. Aucouturier, Structure and physicochemistry of anodic oxide films on titanium and TA6V alloy, Surf. Interface Anal. 27 (1999) 629–637, https://doi.org/10.1002/(SICI)1096-9918(199907)27:7<629:AID-SIA551>3.0.CO;2-0.
[12] V. Zwilling, M. Aucouturier, E. Darque-Ceretti, Anodic oxidation of titanium and TA6V alloy in chromic media. An electrochemical approach, Electrochim. Acta (1999) 921–929, https://doi.org/10.1016/S0013-4686(99)00283-2.
[13] V. Mandić, M. Plodinec, I. Kereković, K. Juraić, V. Janicki, D. Gracin, A. Gajović, A. Moguš Milanković, M.G. Wilinger, Tailoring anatase nanotubes for the photovoltaic device by the anodization process on behalf of microstructural features of titanium thin film, Sol. Energy Mater. Sol. Cells 168 (2017) 136–145, https://doi.org/10.1016/j.solmat.2017.04.028.
[14] L. Sun, S. Zhang, X.W. Sun, X. He, Effect of electric field strength on the length of anodized titania nanotube arrays, J. Electroanal. Chem. 637 (2009) 6–12, https://doi.org/10.1016/j.jelechem.2009.09.023.
[15] J.M. Macak, L.V. Taveira, H. Tsuchiya, K. Sirotna, J. Macak, P. Schmuki, Influence of different fluoride containing electrolytes on the formation of self-organized titania nanotubes by Ti anodization, J. Electroceram. 16 (2006) 29–34, https://doi.org/10.1007/s10832-006-3904-0.
[16] S. Kurajica, J. Macan, V. Mandić, M. Galjer, K. Mužina, J.R. Plaisier, Reinforcing blade-cast photocatalytic-titania film by titanate nanotubes, Mat, Res. Bull. 105 (2018) 142–148, https://doi.org/10.1016/j.materresbull.2018.04.045.
[17] C. Ruan, M. Paulose, O.K. Varghese, G.K. Mor, C.A. Grimes, Fabrication of highly ordered TiO_2 nanotube arrays using an organic electrolyte, J. Phys. Chem. B 109 (2005) 15754–15759, https://doi.org/10.1021/jp052736u.
[18] J. Wang, Z. Lin, Anodic formation of ordered TiO2 nanotube Arrays: effects of electrolyte temperature and anodization potential, J. Phys. Chem. C 113 (2009) 4026–4030, https://doi.org/10.1021/jp811201x.
[19] V.M. Prida, E. Manova, V. Vega, M. Hernandez-Velez, P. Aranda, K.R. Pirota, M. Vazquez, E. Ruiz-Hitzky, Temperature influence on the anodic growth of self-aligned Titanium dioxide nanotube arrays, J. Magn. Magn Mater. 316 (2007) 110–113, https://doi.org/10.1016/j.jmmm.2007.02.021.
[20] G.E. Thompson, Porous anodic alumina: fabrication, characterization and applications, Thin Solid Films 297 (1997) 192–201, https://doi.org/10.1016/S0040-6090(96)09440-0.
[21] G.K. Mor, O.K. Varghese, M. Paulose, N. Mukherjee, C.A. Grimes, Fabrication of tapered, conical-shaped titania nanotubes, J. Mater. Res. 18 (2003) 2588–2593, https://doi.org/10.1557/JMR.2003.0362.
[22] J.M. Macak, H. Tsuchiya, A. Ghicov, K. Yasuda, R. Hahn, S. Bauer, P. Schmuki, TiO2 nanotubes: self-organized electrochemical formation, properties and applications, Curr. Opin. Solid State Mater. Sci. 11 (2007) 3–18, https://doi.org/10.1016/j.cossms.2007.08.004.
[23] L.V. Taveira, J.M. Macák, H. Tsuchiya, L.F.P. Dick, P. Schmuki, Initiation and growth of self-organized TiO_2 nanotubes anodically formed in NH4F/(NH4)2SO4 electrolytes, J. Electrochem. Soc. 152 (2005), https://doi.org/10.1149/1.2008980. B405–B410.
[24] S.P. Albu, A. Ghicov, S. Aldabergenova, P. Drechsel, D. LeClere, G.E. Thompson, J. M. Macak, P. Schmuki, formation of double-walled TiO2 nanotubes and robust anatase membranes, Adv. Mater. 20 (2008) 4135–4139, https://doi.org/10.1002/adma.200801189.
[25] M. Yurddaskal, T. Dikici, S. Yildirim, M. Yurddaskal, M. Toparali, E. Celik, Fabrucation and characterization of nanostructured anatase TiO_2 films prepared by electrochemical anodization and their photocatalytic properties, J. Alloys Compd. 651 (2015) 59–71, https://doi.org/10.1016/j.jallcom.2015.08.064.
[26] Q. ZhangH. Zhou, M. Yang, X. Tang, Q. Hong, Z. Yang, S. Liu, J. Chen, G. Zhou, C. Pan, Fabrication and formation mechanism of gradient TiO_2 nanotubes via bipolar anodization, J. Electroanal. Chem. 915 (2022), 116337, https://doi.org/10.1016/j.jelechem.2022.116337.
[27] A. Ghicov, P. Schmuki, Self-ordering electrochemistry: a review on growth and functionality of TiO_2 nanotubes and other self-aligned MOx structures, Chem. Commun. 20 (2009) 2791–2808, https://doi.org/10.1039/B822726H.
[28] G.K. Mor, O.K. Varghese, M. Paulose, C.A. Grimes, A self-cleaning, room-temperature titania-nanotube hydrogen gas sensor, Sens. Lett. 1 (2003) 42–46, https://doi.org/10.1166/sl.2003.013.
[29] M. Paulose, O.K. Varghese, G.K. Mor, C.A. Grimes, K.G. Ong, Unprecedented ultrahigh hydrogen gas sensitivity in undoped titania nanotubes, Nanotechnology 17 (2006) 398–402, https://doi.org/10.1088/0957-4484/17/2/009.
[30] P. Acevedo-Pena, L. Lartundp-Rojas, I. Gonzalez, Effect of water and fluoride content on morphology and barrier layer properties of TiO_2 nanotubes grown in ethylene glycol-based electrolytes, J. Solid State Electrochem. 17 (2013) 2939–2947, https://doi.org/10.1007/s10008-013-2212-2.
[31] A. Valota, D. LeClere, P. Skeldon, M. Curioni, T. Hashimoto, S. Berger, J. Kunze, P. Schmuki, G. Thompson, Influence of water content on nanotubular anodic titania formed in fluoride/glycerol electrolytes, Electrochim. Acta 54 (2009) 4321–4327, https://doi.org/10.1016/j.electacta.2009.02.098.
[32] D. Regonini, A. Satka, A. Jaroenworaluck, D.W.E. Allsop, C.R. Bowen, R. Stevens, Factors influencing the surface morphology of anodized TiO_2 nanotubes, Electrochim. Acta 74 (2012) 244–253, https://doi.org/10.1016/j.electacta.2012.04.076.
[33] Y. Sun, Q. Zhao, G. Wang, K. Yan, Influence of water content on the formation of TiO_2 nanotubes and photoelectrochemical hydrogen generation, J. Alloys Compd. 711 (2017) 514–520, https://doi.org/10.1016/j.jallcom.2017.03.007.
[34] K. Raja, T. Gandhi, M. Misra, Effect of water content of ethylene glycol as electrolyte for synthesis of ordered titania nanotubes, Electrochem. Commun. 9 (2007) 1069–1076, https://doi.org/10.1016/j.elecom.2006.12.024.
[35] L.M. Peter, D.J. Blackwood, S. Pons, Photocorrosion of n-Si in ammonium fluoride solutions: an investigation by in-situ Fourier transform infrared spectroscopy, J. Electroanal. Chem. Interfacial Electrochem. 294 (1990) 111–121, https://doi.org/10.1016/0022-0728(90)87139-B.
[36] F.S. Talatori, S. Fatemi, A. Nouralishahi, Impact of butanol and ammonium fluoride on synthesizing and optical properties of N-doped carbon dots, Solid State Sci. 97 (2019), 105988, https://doi.org/10.1016/j.solidstatesciences.2019.105988.
[37] R.R. Bacsa, M. Gratzel, Rutile formation in hydrothermally crystallized nanosized titania, J. Am. Ceram. Soc. 79 (1996) 2185–2188, https://doi.org/10.1111/j.1151-2916.1996.tb08956.x.
[38] Y. Zhang, X. Ma, P. Chen, D. Yang, Effect of the substrate temperature on the crystallization of TiO_2 films prepared by DC reactive magnetron sputtering, J. Cryst. Growth 300 (2007) 551–554, https://doi.org/10.1016/j.jcrysgro.2007.01.008.
[39] R.M. Arán-Ais, E. Herrero, J.M. Feliu, The breaking of the C\C bond in ethylene glycol oxidation at the Pt(111) electrode and its vicinal surfaces, Electrochem. Commun. 45 (2014) 40–43, https://doi.org/10.1016/j.elecom.2014.05.008.
[40] H. Okamoto, W. Kon, Y. Mukouyama, Five current peaks in voltammograms for oxidations of formic acid, formaldehyde, and methanol, on platinum, J. Phys. Chem. B 109 (2005) 15659–15666, https://doi.org/10.1021/jp0516036.

[41] N. Seselj, C. Engelbrekt, Y. Ding, H.A. Hjuler, J. Ulstrup, J. Zhang, Tailored electron transfer pathways in aucore/ptshell–graphene nanocatalysts for fuel cells, Adv. Energy Mater. 8 (2018), 1702609, https://doi.org/10.1002/aenm.201702609.
[42] N.W. Maxakato, K.I. Ozoemena, C.J. Arendse, Dynamics of electrocatalytic oxidation of ethylene Glycol,Methanol and formic acid at MWCNT platform electrochemically modified with Pt/Ru nanoparticles, Electroanalysis 22 (2010) 519–529, https://doi.org/10.1002/elan.200900397.
[43] C. Jin, Y. Song, Z. Chen, A comparative study of the electrocatalytic oxidation of ethylene glycol on PtAu nanocomposite catalysts in alkaline, neutral and acidic media, Electrochim. Acta 54 (2009) 4136–4140, https://doi.org/10.1016/j.electacta.2009.02.054.
[44] A. Nemcova, I. Kubena, M. Šmid, H. Habazaki, P. Skeldon, G.E. Thompson, Effect if current density and behaviour of second phases in anodizing of a Mg-Zn-RE alloy in a fluoride/glycerol/water electrolyte, J. Solid State Electrochem. 20 (2016) 1155–1165, https://doi.org/10.1007/s10008-015-2864-1.
[45] Y. Lai, J. Gong, C. Lin, Self-organized TiO_2 nanotube arrays with uniform platinum nanoparticles for highly efficient water splitting, Int. J. Hydrogen Energy 37 (2012) 6438–6446, https://doi.org/10.1016/j.ijhydene.2012.01.078.